SIMULATION OF A CCD STAR TRACKER

E. M. Winter and D. P. Wisemiller
International Business Machines Corporation
2625 Townsgate Road
Westlake Village, California 91361

ABSTRACT

With the availability of lightweight solid-state imaging devices, such as Charge Coupled Devices (CCDs), it is feasible to consider wide field-of-view star trackers for spacecraft guidance and navigational functions. For this application, the star tracker will detect and match a pattern of many stars. However, because the image plane of a CCD is quantized, each star image will fall on many individual detectors. In addition, with some CCD devices (interline transfer devices), opaque areas exist in the focal plane. In this paper a general purpose electro-optical sensor simulation is described. This simulation utilizes the convolution approach to optical simulation rather than the Fourier transform approach. This approach offers several computer run-time and flexibility advantages. One feature of this simulation is a large, stored preconvolution table representing the convolution of a unit point source and the optics/detector. The charge transfer effect, inherent in CCDs, is also simulated. The application of this simulation to a CCD star tracker application is discussed. Also, results determining the detector-limited resolution for several focal plane geometries are presented. This resolution is determined by simulating the convolution of the star with the optics, the detector grid, and the charge transfer readout. This simulated sensor data stream is then input to centroiding and thresholding algorithms, and the calculated position is compared to the input star locations.

INTRODUCTION

Charge Coupled Devices (CCDs) are being considered for a wide range of electro-optical applications. Typical applications include optical character recognition, commercial television, surveillance, point-of-sale terminals, and scientific instruments. CCD applications can be broadly grouped into two categories: applications with and without signal or data processing. While simulation is of value for both categories, it is most useful for applications where the device output is subsequently processed. In this paper, the digital computer simulation of a Charge Coupled Device star tracker and associated processing is discussed. The advantages of a simulation approach to determine CCD accuracy are treated. While the emphasis of this paper is on the description of the simulation, a summary of simulation experiment results is included.

A star tracker is necessary for the function of spacecraft guidance and navigation. With present photomultiplier tube star trackers, the signal of a single reference star is used. Deviations from nominal orientation are noted as changes in the output voltage from the star tracker. A CCD star tracker operates on a different principle. Because a CCD is a two-dimensional mosaic of detector cells, the images of many stars can be acquired simultaneously. The relative orientation of the pattern of stars can then be compared to an inertial pattern, available from a standard star catalog. An example of this pattern matching function is shown in Figure 1.

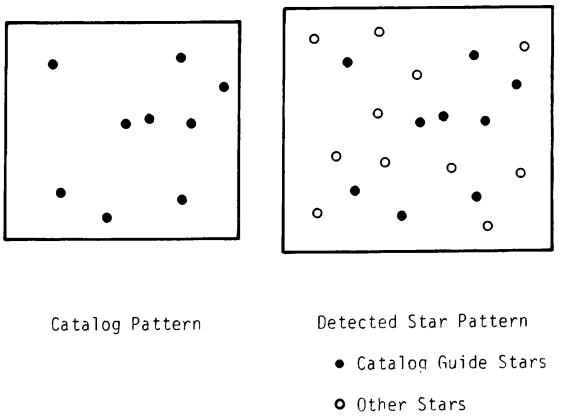

Figure 1. Star Pattern Recognition Concept

A Charge Coupled Device offers many advantages over present star tracking devices. Since it is a solid state device, it is inherently less bulky than a photomultiplier tube. (For a full discussion of the advantages of CCDs, see Reference 1.) With decreased spacecraft vehicle impact potential, in terms of size, weight, and power, it is important to examine the possible accuracy of the pattern recognition concept. The accuracy of this concept has been examined from an analytical viewpoint in Reference 1. Because of the complexity of the problem, an examination in greater detail using simulation was warranted.

SIMULATION VERSUS ANALYTICAL APPROACH

In the solution of system problems, the system designer must often decide between a purely analytical approach and a simulation approach. A consideration of the complexity and ultimate usefulness of an analytical approach is necessary. While a simulation may need verification, the assumptions inherent in analysis require justification. Also, the influence of random processes must be studied. When several random processes are interacting, a simulation is normally much better suited for problem solving. The subjective appeal of a simulation may be important. A simulation introducing a high degree of realism when coupled with computer graphics techniques can be an effective demonstration vehicle. Finally, the simulation is available during the development cycle to produce test data and drive signal processing functions.

The determination of the performance of pattern trackers can be divided into two problems. The first problem is the determination of the inherent accuracy in the observa- of single stars. The second problem is the determination of how that inherent accuracy translates into actual system accuracies.

The inherent accuracy of single star observations is dependent upon the spatially quantized nature of the detector grid, the optical blurring (or point spread), the position of the star, and the system noise characteristics. The first two effects are illustrated in Figure 2. The finite resolution of the optical system turns the image of a point source into an extended two-dimensional image. For simplicity, this can be represented as a two-dimensional Gaussian in x and y (the detector coordinates). This extended image is collected in the discrete detectors of the CCD detector grid. As a result, the smooth Gaussian image becomes a quantized approximation. The problem of determining the inherent accuracy of the CCD star tracker can then be stated simply: Using this two-dimensional sampled Gaussian, how accurate are potential interpolation schemes in determining the location of the center of the Gaussian (the actual star equivalent location). The last two effects, star location and system noise, complicate the problem further. In the example shown in Figure 2, the star was shown located in the center of a detector resolution cell. However, in general,

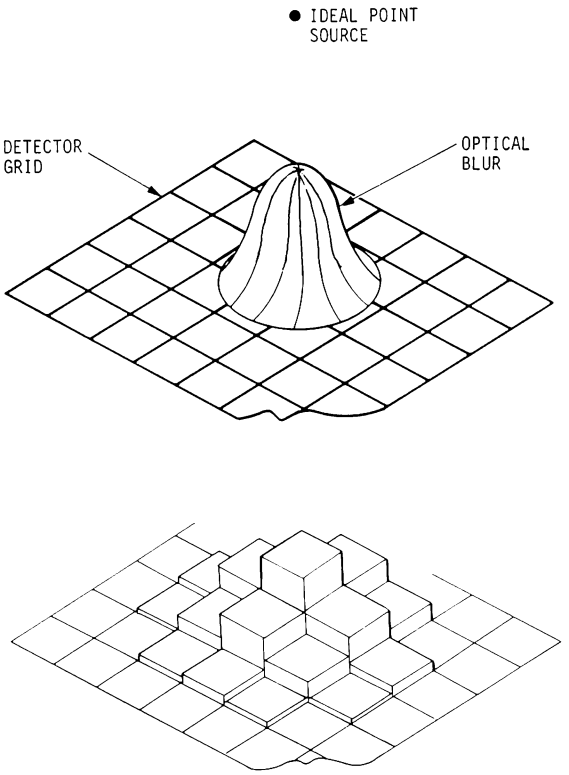

Figure 2. Optical and Detector Effects on an Ideal Point Source

the star may be located with equal probability at any position in a cell. Two examples of other locations are shown in Figure 3. In case 1, the star is located at the edge of a cell and the detector response is nearly equally partitioned between two cells. In case 2, the response is split between four cells.

The inherent accuracy of a star tracker as a function of star location can be calculated for any position in the cell for the above three effects. It is the fourth effect, system noise, which makes analysis difficult. The energy collected in each CCD detector cell is randomly perturbed by noise. These perturbed energies are then subject to thresholding. Thresholding is described in greater detail in a later section. The interaction between the random noise and thresholding can easily eliminate one or more of the cell responses shown in Figures 2 and 3. With the loss of one or more cells, the interpolation scheme will inaccurately estimate the centroid (image center). Because noise is a random process, it is best handled through simulation.

The output of the inherent accuracy study is the centroiding accuracy as a function of star position (in a cell) and intensity for a given system. This can be used to select the intensity of the guide stars. These accuracies, determined from the controlled experiment discussed above, must be verified for a realistic observational environment. For this case, a simulated star field with stars

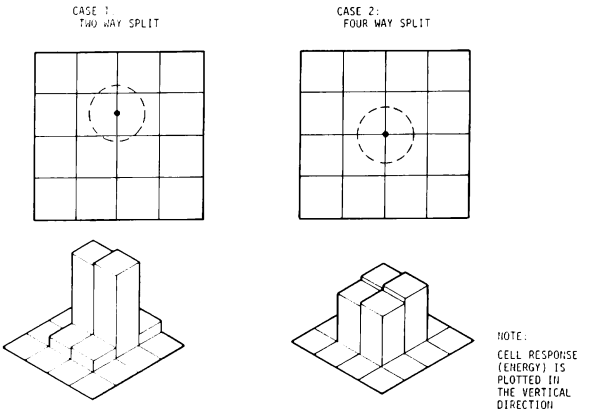

Figure 3. Effect of Star Location on Energy Distribution

characteristic of the celestial spere is needed. Only a simulation can fully answer this question.

In the next section, the characteristics of the simulation used to evaluate the CCD star tracker are described. The simulation of a CCD star tracker was just one of several potential applications of that simulation and great emphasis was placed on flexibility and run-time economy.

CCD SENSOR SIMULATION

Overview

In general, a CCD sensor system consists of the following components: object or input signal, optics, the CCD detector grid, readout, and signal processing algorithms (see Figure 4). The light from an object is collected by the optics and imaged onto the CCD detector grid. The image is then read out by transferring the charge. Following detection and readout, the output of the CCD may be subjected to processing algorithms. In this section, the simulation of an image through the signal processing stage will be examined. This simulated image data stream is then used to evaluate the effectiveness of star tracker interpolation algorithms.

Two techniques for simulation implementation were evaluated: direct convolution and a method utilizing Fourier transforms. A tradeoff of these two techniques is discussed in Reference 2. These two techniques were examined from the viewpoint of computer efficiency, accuracy, and ease of implementation for the purpose of developing a large scale electro-optical simulation. With the increase in the size of simulations, the trend has been toward Fourier techniques because of their computer efficiency. It was found, for the image and system being simulated, that the direct convolution technique offered a significant run-time advantage. For the specific case of simulation of a star field image, the run-time advantage of direct convolution is even greater than that discussed in Reference 2.

The overall functional flow of the sensor system simulator is shown in Figure 5. This simulation was implemented based upon this model of direct convolution of image transducer and optics. The first step in the process is to produce an equivalent point source image.

Star Generation

For the simulation of a CCD star tracker, digitization of a photographic image can be avoided and the equivalent point source image generated by two methods. First, the option exists to generate stars using random numbers. Three random numbers are used to generate the focal plane x and y coordinates and the star intensity. The number of stars is

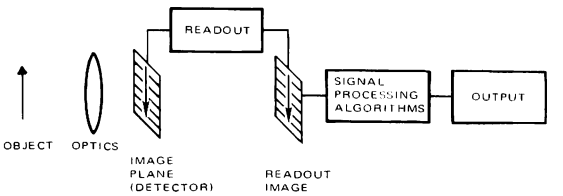

Figure 4. Components of a CCD Sensor System

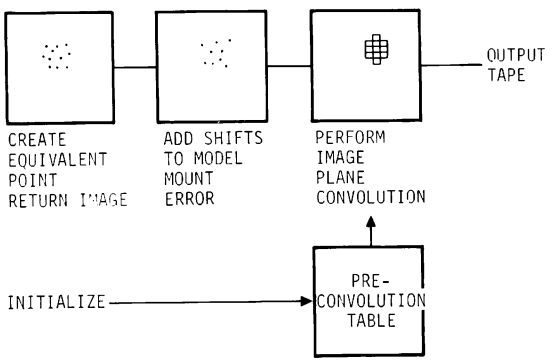

Figure 5. Functional Flow of Sensor System Simulation

selected by specifying a star generation intensity threshold and the selected portion of the celestial sphere. Stars are created with a continuum of intensities above this threshold at densities corresponding to the area of the sky simulated. Also present is the capability to use a star catalog. Stars of magnitude 9.5 or brighter can be generated from a digital tape of the Smithsonian Astrophysical Observatory (SAO) Catalog (Reference 3). This catalog contains approximately 260,000 stars and is available on computer compatible tape (Reference 4). Of the information present on the catalog tape, only the right ascension-declination and magnitude are utilized for the simulation. These inertial coordinates must be transformed into detector coordinates to create observations of the cataloged stars. If stars of magnitude 9.5 or dimmer are required, both random number techniques and the catalog must be utilized because the SAO catalog is not complete below magnitude 9.5. The resulting simulated star field contains catalog stars for guidance and navigational purposes as well as a representative star population to any desired magnitude level.

Following simulation of possible image motion, the ideal points are convolved with the optics and the detector. Finally, the point returns are replaced by a matrix of cell returns.

Convolution Modelling

The convolution technique, as implemented, is separated into two steps: an initialization phase, performed only once for any set of sensor system parameters, and the processing phase, performed once for each image source in the picture using the table. In this section, the method of simulation utilizes the convolution approach, and the formation of the preconvolution table for a general CCD sensor is discussed.

The convolution approach to electro-optical simulation involves the direct solution of the convolution integral which describes the intensity in the image plane at position x, y:

$$I(x,y) = \int_{-\infty}^{\infty} \int_{-\infty}^{\infty} I(x',y')\, f(x-x',\, y-y')\, dx'dy' \qquad (1)$$

(Reference 5)

where I(x',y') is the intensity distribution function of an idealized image at the image plane and f(x->', y-y') is the point spread function of the optics.

Equation (1) can be easily integrated for the case of a point source. To include the finite resolution of the detector grid, the intensity given by equation (1) must be integrated over the resolution cell (i,j):

$$I(i,j) = \int_{x=a}^{x=b} \int_{y=c}^{y=d} I(x,y)\, w(x,y)\, dydx \qquad (2)$$

where w(x,y) is the responsivity of the resolution cell as a function of position, and a, b, c, and d are the limits of the responsive area of the cell in x and y, respectively.

For the case of a real extended image function I(x', y'), the integration of Equation (2) would be extremely difficult. However, it is possible to make some simplifications to the problem because of the finite resolution of the detector grid. If the sensor can be assumed to be linear and shift invariant, the real extended ideal image can be broken into equivalent point sources and Equation (2) restated:

$$I(i,j) = \sum_{K} \int_{x=a}^{x=b} \int_{y=c}^{y=d} I_k\, f(x-x_k,\, y-y_k)\, w(x,y)\, dydx \qquad (3)$$

where I_k is the intensity of the kth equivalent point source located at position x_k, y_k in the image plane.

Equation (3) thus gives the light deposited on cell (i,j) by all point sources (sum over k). There may be 100,000 or more resolution elements and four times as many point source equivalents (based upon a 1/2 cell minimum spacing), therefore, the operations represented by Equation (3) are not trivial.

In the approach implemented for this simulation, a method of preconvolving the equivalent point sources and storing this preconvolution was developed. Since convolution integrations in the main line of the sensor simulation can be avoided, this approach represents a significant time saving. To precalculate the convolution integral (Equation (3)), the fundamental geometry of the sensor was defined as the area over which the point spread function has non-zero value (physical dimensions of the optical blur). The convolution integration can then be performed for this fundamental geometry only. The result of this process is a table which represents the digital point spread function for possible positions in a CCD cell.

In the following paragraphs, the table initialization for a simple solid state imaging sensor is discussed. To simplify the problem, the sensor plane responsivity function w(x,y) is defined to be unity within each cell. Also, the cell is assumed to be, in general, rectangular with a rectangular sensitive area. With these assumptions, the responsivity function can be included in the limits of the integration:

$$I'(i,j) = \int_{x_1-a_1}^{x_1+a_2} \int_{Y_m-b_1}^{Y_m+b_2} f(x-x_0,\, y-y_0)\, dy\, dx \qquad (4)$$

where for the fundamental geometry, (x_0,y_0) can be set at the origin and a_1, a_2, b_1, b_2 define the extent of the sensitive area as measured from cell center (see Figure 6).

For simplicity, a two-dimensional Gaussian point spread function is used, and the integration of Equation (4) can then be separated into two one-dimensional integrations:

$$I'(i,j) = \int_{x_1-a_1}^{x_1+a_2} \frac{1}{\sqrt{2\pi\sigma_o}} \exp -\left[\frac{(x-x_o)^2}{2\sigma_o^2}\right] dx$$

$$\int_{Y_m-b_1}^{Y_m+b_2} \frac{1}{\sqrt{2\pi\sigma_o}} \exp -\left[\frac{(y-y_o)^2}{2\sigma_o^2}\right] dy \qquad (5)$$

The above expression will result in the normalized intensity for cell i,j for a point spread function centered at position (x_o, y_o). This equation can be expressed in terms of error functions to result in:

$$I'(i,j) = \left[\text{erf}\left(\frac{x_i+a_2-x_o}{\sqrt{2\sigma_o}}\right) - \text{erf}\left(\frac{x_i-a_1-x_o}{\sqrt{2\sigma_o}}\right)\right]$$

$$\left[\text{erf}\left(\frac{Y_i+b_2-Y_c}{\sqrt{2\sigma_o}}\right) - \text{erf}\left(\frac{Y_i-b_1-y_o}{\sqrt{2\sigma_o}}\right)\right] \qquad (6)$$

Equation (6) is then used to create a large preconvolution table at simulation initialization. This table is then accessed and applied during the main line of the simulation.

Figure 7 illustrates how this table is applied. In this example, an idealized return is located at X = 2.2 and Y = 2.3 in detector coordinates with an intensity of 1000 units. For this illustration, it can be assumed that this is the first point processed, hence the initial value of all the cells is zero intensity. This example is for a 3 cell by 3 cell fundamental geometry with only 6 x 6 subcell values (quantization in the cell).

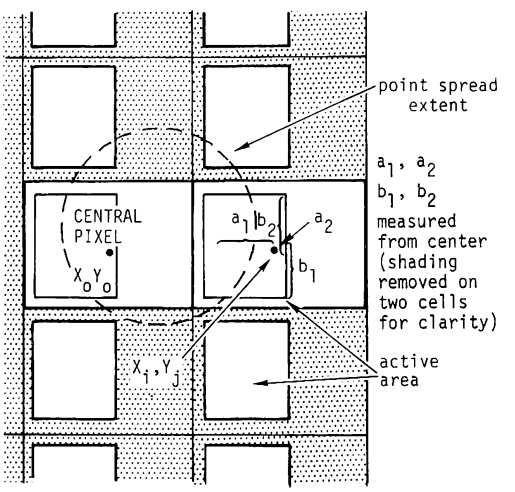

Figure 6. Fundamental Geometry of CCD Detector (shading represents non-responsive area)

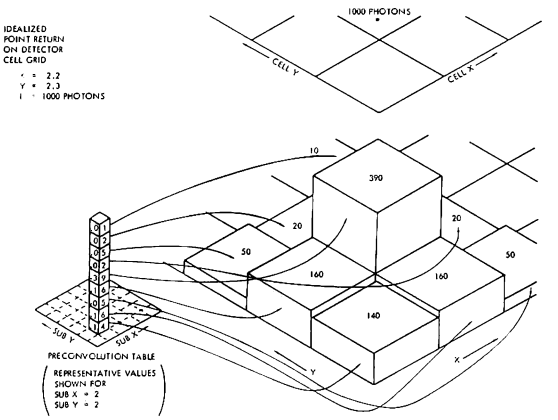

Figure 7. Example of 3 x 3 Preconvolution Table Usage with 6 x 6 Sub-Cell Quantification

The first step in the processing is to determine which sub-cell values to access for the point return. In this example, the point has an X sub-cell value of 0.2 and a Y sub-cell value of 0.3. Because each cell is divided into 6 sub-cells in each direction, it can be seen that this point lies in the second X and second Y sub-cell. These sub-cell values are converted to indices which access the appropriate portion of the table. The preconvolution table is stored as an array with the elements being sub-cell X and Y and the nine table values for the eight neighboring cells and the central cell. Each value represents the fractional portion of the total idealized intensity to be distributed to the corresponding cell. For clarity in the figure, table values are shown for only one sub-cell. Once the proper sub-cell has been identified and table values indexed, each value is multiplied by the point source intensity (1000 units in the example), and the result is added to the existing value for the corresponding cell. For example, the central cell according to the table should receive 39 percent of the total intensity, or 1000 x 39% = 390 units.

For purposes of efficiency, the charge transfer effects of CCDs were simulated as part of this process. Charge transfer is a CCD effect whereby, as part of the readout process, a portion of the signal is left behind. Because this is a linear process, it can be reflected back to the convolution. To simulate charge transfer effects, a small portion of the energy in each cell was shifted to the down channel neighbor. The fraction shifted depended on the cell location.

Examples of the distortion introduced into an otherwise symmetric star point spread image are shown in Figure 8. In example one (10 transfers), the distortion introduced is relatively minor. However, for the second example (170 transfers), the distortion is major. This effect, while predictable, is present in all CCDs and must be considered in any star tracker interpolation algorithm.

Following the application of the image plane convolution process, the signal for each cell is subjected to a noise application process. Besides charge transfer effects, the CCD is subjected to several random noise processes which can be characterized as signal dependent and signal independent. Signal dependent noise is Poisson noise caused by fluctuations in the number of photons collected during the integration period. The variance of this noise source is equal to the actual collected electron count in each individual cell. The signal independent noise is caused by thermal processes. These two noise variances are calculated and summed for each cell, and the variances input to a Gaussian random number generator to calculate the noise perturbed signal for each cell.

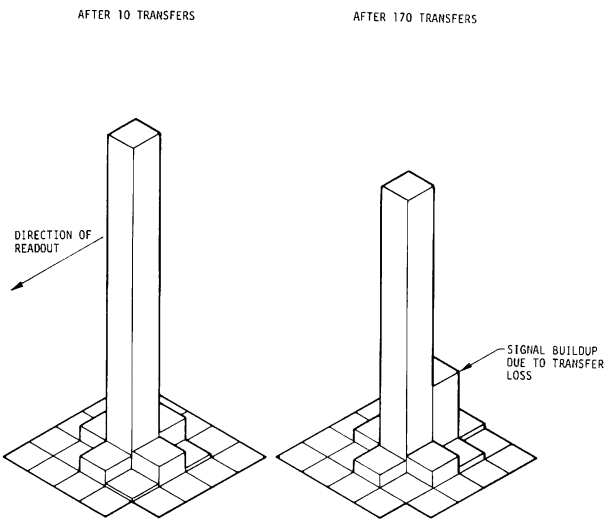

Figure 8. Charge Transfer Alteration of Point Spread Function

The simulated data at this point represents the output of a CCD imager and associated circuitry. This data is then fed into applicable signal processing algorithms for determining the centroids of selected stars.

STAR TRACKER PROCESSING CONCEPTS

The important star tracker algorithms for simulation evaluation are those which perform thresholding and centroiding operations. Subsequent algorithms for calculation of the actual spacecraft platform deviation angles can be evaluated analytically, once the fundamental focal plane errors have been determined. In this section, candidate star tracker algorithms are discussed.

The star tracker concept uses a catalog of selected guide stars. These stars are selected for coverage of areas of the celestial sphere where viewing is anticipated. The intensity of guide stars is selected within the intensity range suggested by the inherent accuracy study. The predicted position of the guide stars in the focal plane is calculated and a search area specified for each star. The size of this search area is determined by estimates of the possible satellite platform errors. The data in each m x n cell search area is then processed independently. The flow of the processing of a star tracker image is shown in Figure 9.

The first function to be performed is thresholding. In the thresholding function, cells with energy below a preset level are set to zero. The value of the calculated threshold depends upon the estimate of the total background level. For a CCD star tracker, this background principally comes from internally generated dark charge, although such external sources as the zodiacal light may contribute. In a dark charge limited device, the threshold will be a function of position within the array and not a function of the area of the sky observed. In this case, the threshold is calculated using:

$$T(i,j) = B(i,j) + T\sqrt{B(i,j) + \sigma^2}$$

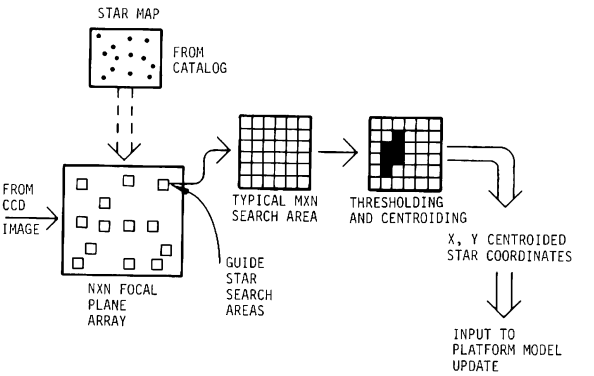

Figure 9. Overall Flow of Star Tracker Signal Processing

where

$T(i,j)$ is the threshold for cell i,j

$B(i,j)$ is the background as a function of position

T is a preset signal to noise ratio (at least 3 to minimize false noise exceedences)

σ^2 is the variance of the signal independent noise

This array of numbers for the threshold matrix can be prestored.

Following thresholding, two processing options exist: interpolation using intensity and interpolation without intensity. From a signal processing point of view, the second option is simpler, because no intensity information is required past the thresholding function. For option 1 (no intensity) the centroids are calculated using:

$$\bar{X} = \frac{\Sigma X_i}{N}$$

$$\bar{Y} = \frac{\Sigma Y_i}{N}$$

where X_i, Y_i are the individual cell positions and N is the number of cells centroided.

For option 2, the intensity values should be corrected for the predicted smearing due to charge transfer. After intensity correction (position dependent) for each point above threshold, the centroids are calculated using:

$$\bar{X} = \frac{\Sigma X_i (I_i - B)}{N \times \Sigma (I_i - B)}$$

$$\bar{Y} = \frac{\Sigma Y_i (I_i - B)}{N \times \Sigma (I_i - B)}$$

where B is the background and I_i are the individual cell intensities.

The above algorithms were coded for simulation evaluation. The data stream produced by the sensor simulation was then input to both of these algorithms. To determine inherent accuracy as a function of position, intensity, etc., input star positions were compared to the output centroids.

SIMULATION EXPERIMENT RESULTS

In a previous section, two different experiments were postulated. The first was the measurement of the inherent accuracy of the centroiding operation. The results of this experiment would serve as a basis of a system design. In the second experiment, candidate system designs would be tested against realistic star fields. The second set of experiments are still in the formulation stage. In this section, some results of the inherent accuracy study will be presented. Also, the capability of the simulation to perform the second set of experiments will be demonstrated.

The key question for the inherent accuracy study is the measurement of the error introduced through the optics and the detector. Two optical blur models (point spread functions) were input: a "large" point spread function with Gaussian radius equal to the CCD cell width and a "small" point spread function with Gaussian radius equal to 0.3 times the cell width. These point spread functions are shown in Figure 10 for the case where the star is centered in a cell. These two optics models were used to produce two simulated data streams. The output of these data streams was input into the two centroiding options discussed above.

To evaluate the options, a controlled experiment was performed. Twenty stars of five different intensity levels were generated at prespecified positions. Five different exposure data frames were created with the stars all in the positions indicated in Figure 11. Thus, all 100 stars in exposure 1 were placed in the center of their respective cells. These ideal stars were then sent through the two different optics models. Noise was then applied and the data evaluated using the two centroiding options. The experiment matrix consisted of: five different positions, two optical point spread functions, five star intensity levels, and two centroiding options. The goal was to determine the inherent accuracy (position dependency) of each centroiding option as a function of blur radius and star intensity. A recommendation for star tracker parameters would be based upon the results.

To verify the accuracy of the simulation in this controlled experiment, a single star placed in position 4 (of Figure 11) was traced through the convolution and centroiding processes. This verification is shown graphically in Figure 12. In the top portion of Figure 12, the convolved energy for a star of 1675 electrons is shown for the two-point spread functions under study. The portion of the image above threshold is shaded. Note that three cells are above threshold for case a and five for case b. Below the convolved energy diagrams is the result of the centroiding operation for intensity weighted and geometric centroiding. The calculated positions are compared to the true position.

It was found that of the five star positions shown in Figure 11, position 4 was the most useful in determining the inherent accuracy as a function of intensity for a given optics/centroiding combination. The results obtained from experiments with positions 1, 2, and 3 tended to favor the

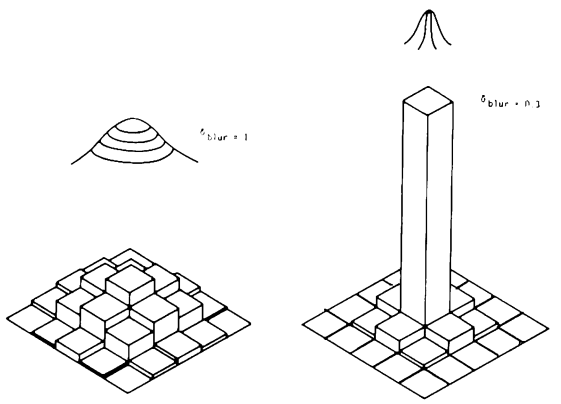

Figure 10. Large and Small Blur Examples

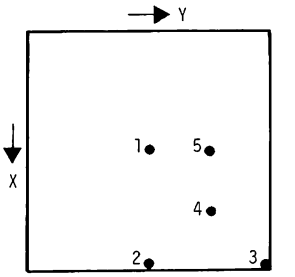

Position	Deviation from Cell Center δX	δY
1	0	0
2	.5	0
3	.5	.5
4	.25	.25
5	0	.25

Figure 11. Controlled Star Positions

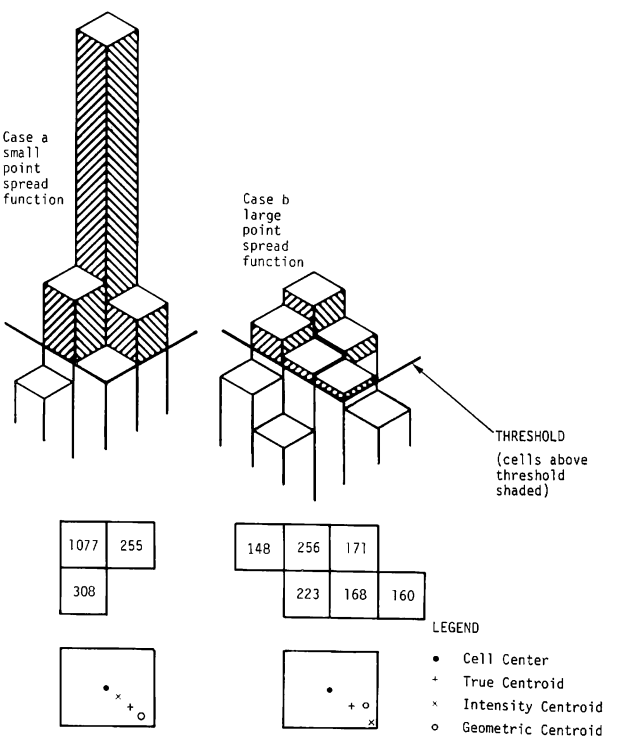

Figure 12. Typical Star Histories

geometric centroiding option. This is to be expected since these positions are easily estimated using 1, 2, and 4 cells above threshold.

For example, in position 1 (star centered in the cell), the inherent accuracy was worse for the dimmest and brightest stars. The error in the star position was caused in each case by noise. For the dim star case, noise occasionally resulted in a cell other than the nominally brightest cell occurring above threshold. For the bright star case, noise caused one or more of the fringe cells to exceed threshold in addition to the central cell.

The accuracy results for position 4 are shown in Figure 13. The average error is plotted as a function of star intensity for the four configurations discussed above. The abscissa is the signal-to-noise ratio of the star expressed as:

$$S/N = \frac{I}{\sqrt{B + \sigma^2}}$$

where I is the intensity of the star measured in electrons. This intensity is the sum of all electrons produced in the detector array by the light from the star. It is interesting to note that there is a significant improvement for all cases as intensity increases. This is to be expected; however, the accuracy curves do not flatten until a signal-to-noise ratio of nearly 20. The curves depicting the standard deviation of the accuracy error show a similar property.

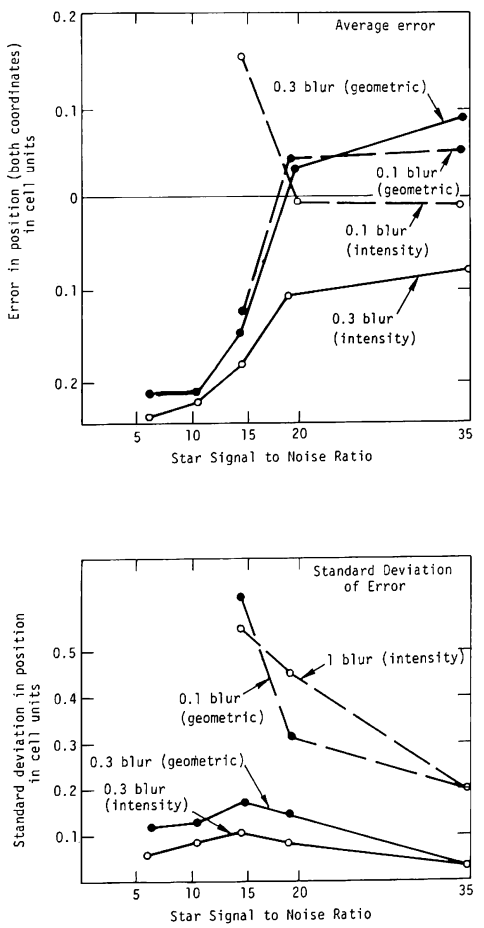

Figure 13. Inherent Accuracy Results

In general, the wider point spread function resulted in greater accuracy than the narrow. Greater accuracy is also obtained with intensity centroiding. The standard deviation results point toward an interesting system trade-off. In general, the standard deviation of the errors produced using the smaller point spread function are much less than those from the larger point spread function. Because the standard deviation is related to the number of samples which must be taken to ensure a particular accuracy, a system designed with a small point spread function will require fewer stars. This has significant impact on the overall system design. Overall, however, a system with a relatively large point spread function and intensity weighted centroiding is recommended.

The capability of the simulation to produce a realistic star field was demonstrated through use of a photoscanner. The output of a simulated star field was converted to gray levels. The photoscanner was then used to produce a negative by exposing a small portion of the film for each cell of simulated data.

The photographic output of a simulated realistic star field is shown in Figure 14. The figure is a negative image with black corresponding to high intensity. The stars in this image were produced using random numbers. At the same time the simulated stars were generated, a pseudo-catalog of guide stars was produced. These guide stars in this catalog are referenced to their ideal focal plane positions and can be used to center searches in the simulated images. While the stars in Figure 14 do not bear any relation to real star patterns, a true catalog could be substituted for the random generation. In future work, the inherent accuracy results will be investigated using realistic star fields.

SUMMARY

An accurate general purpose CCD sensor simulation was developed and applied to the specific case of a CCD star tracker. A recommendation as to system configuration was made. A relatively large point spread function coupled with intensity weighted centroiding is preferred. However, if small field-of-view star trackers are necessary, a smaller point spread function would be preferred. The capability of the simulation to model realistic star fields was described.

ACKNOWLEDGEMENTS

The authors were aided in the work reported in this paper by a number of people including J. Falkner, R. Gormley, K. Klementis, G. Loffredo, and J. Ujihara.

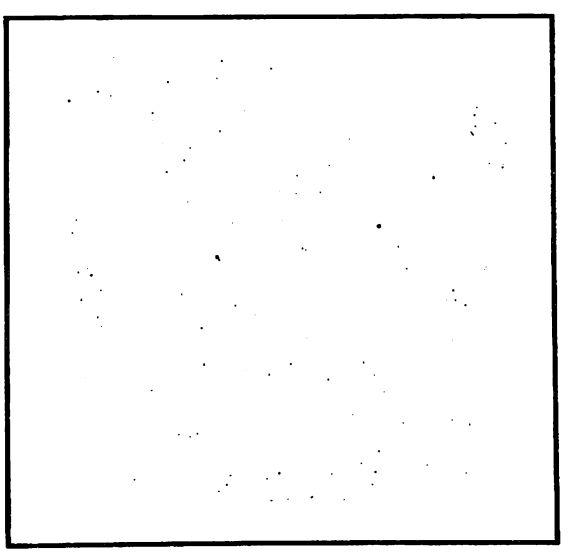

Figure 14. Simulated Star Field

REFERENCES

1. Goss, W. C., "CCD Star Trackers," Proceedings Symposium on Charge-Coupled Device Technology for Scientific Imaging Applications, JPL SP 43-21, Jet Propulsion Laboratory, Pasadena, Ca., 1975.

2. Winter, E. M. and Wisemiller, D. P., "Development of a Large-Scale Electro-Optical Simulation," Proceedings of the Society of Photo-Optical Instrumentation Engineers, Vol. 59, pp. 183-193, 1975.

3. Staff of the Smithsonian Astrophysical Observatory (SAO), Star Atlas of Reference Stars and Non-Stellar Objects, MIT Press, Cambridge, Mass., 1969.

4. Haramundanis, K. L., "SAO Star Catalog Tapes," Smithsonian Institution Astrophysical Observatory, Report 705-10, 1967.

5. Papoulis, A., Systems and Transforms with Applications to Optics, McGraw-Hill, New York, 1968, pp. 13-16.